Power Electronic Systems
Laboratory

Proceedings of the 16th Annual IEEE Energy Conversion Congress and Exposition (ECCE 2024), Phoenix, AZ, USA, October 20-24, 2024

Advanced Control of Modularized Bridge Rectifier Solid-State Transformers in MVAC-LVDC Applications

G. Andrioli,
S. Calligaro,
J. Huber,
J. W. Kolar,
R. Petrella

ETH zürich

Advanced Control of Modularized Bridge Rectifier Solid-State Transformers in MVAC-LVDC Applications

Giacomo Andrioli*, Sandro Calligaro*, Jonas Huber†, Johann W. Kolar†, and Roberto Petrella*
*PEMD Laboratory, DPIA, University of Udine, Italy
†Power Electronic Systems Laboratory, ETH Zurich, Switzerland

***Abstract*—Solid-state transformers (SSTs) enable the interfacing of medium-voltage (MV) ac grids to low-voltage (LV) dc loads with high power density and advanced power flow control over traditional approaches based on low-frequency transformers (LFTs). The modularized bridge rectifier (mBR) is a promising, yet understudied, topology which has been recently proposed for high-power electric vehicle (EV) charging applications. The mBR is essentially composed of a three-phase diode rectifier with isolated dc-dc converters connected in parallel to the series-connected diodes, thus forming six branches; the LV outputs of the isolated dc-dc converters are connected in parallel to the LVdc port. In this paper, the mBR SST and its operating principle are first recalled along with an in-depth analysis of the state-of-the-art branch-oriented current control method, which, however, cannot adequately handle the inherent coupling between the branches. Thus, a novel ΣΔ-Vector modeling and control method is proposed, which is based on the Clarke transform and a subsequent ΣΔ decoupling to treat the sums (Σ) and differences (Δ) of the branch quantities separately. The two corresponding equivalent circuits contain only the four effectively available degrees of freedom the mBR topology offers, and hence facilitate a clear analysis and a straightforward, decoupled controller design. Finally, the novel ΣΔ-Vector control method is validated by means of circuit simulations of a 1-MW, 10-kV case study system, and found to show better dynamic performance and robustness than the conventional branch-oriented control method.**

***Index Terms*—Modularized bridge rectifier, solid-state transformer, control, medium voltage, power electronic transformer.**

I. Introduction

An increasing number of power conversion systems demand high flexibility and high power density when interfacing with a medium-voltage (MV) grid, both when directly connecting a load and when interfacing another grid, e.g., a low-voltage (LV) one, [1]. As low-frequency transformer (LFT) based solutions do not fulfill these requirements, medium-frequency transformers [2] and power electronic stages [3] have been combined to form so-called solid-state transformers (SSTs) [4]. Throughout the years, SSTs gained attention in a wide variety of applications, e.g., renewable energy and smart grids (photovoltaic and wind power plants, energy transmission and control) [1], sustainable mobility (railway and ultra-fast electric vehicle (EV) charging) [5]–[10], data centers [11], and large-scale hydrogen electrolyzers [12]–[14].

This publication was co-financed by the European Union (EU) - FSE, PON Ricerca e Innovazione 2014-2020, Italian Ministry of University and Research.

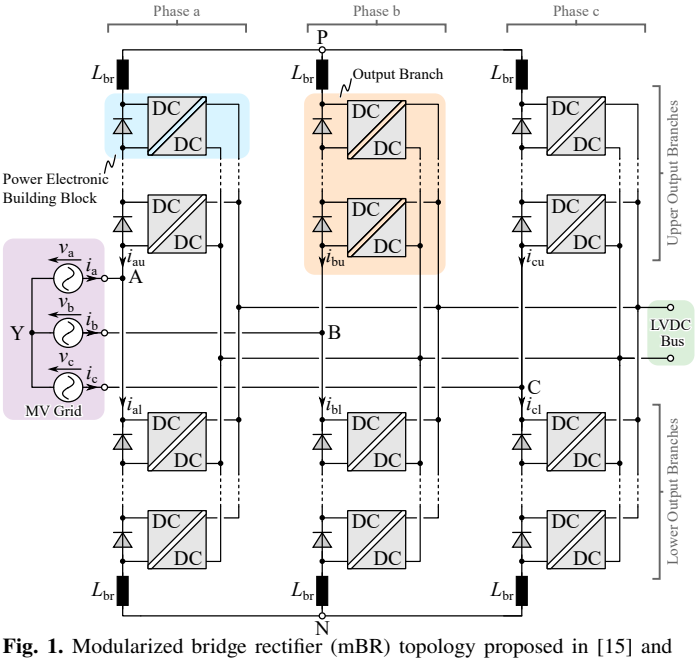

Fig. 1. Modularized bridge rectifier (mBR) topology proposed in [15] and analyzed in [16]; dc-dc converters in parallel to blocking diodes transfer power between the medium-voltage (MV) ac grid and the low-voltage (LV) dc load.

However, the maturity of LFT technology expresses itself mainly in high reliability and low cost, [4], which, despite substantial improvements, slows down a wider adoption of SSTs. To mitigate the price disadvantage, modularity is a highly desirable feature; indeed, most SST topologies are phase-modular, i.e., each MV phase connects to an input-series, output-parallel (ISOP) arrangement of power electronic building blocks (PEBBs), each containing an ac-dc and an isolated dc-dc converter stage [3]. Nonetheless, each PEBB processes a single-phase power flow with a corresponding pulsation at twice the mains frequency. Instead, an MVac-facing unfolder stage could be employed such that the PEBBs must only provide isolated dc-dc conversion; this concept can be employed to individual phases [17], or, advantageously, a three-phase unfolder stage, i.e., a three-phase diode rectifier, is used [18]–[20].

Alternatively, the isolated dc-dc converters could be integrated into the branches of a three-phase diode rectifier, resulting in the modularized bridge rectifier (mBR) as reported in **Fig. 1**. The rectifier diodes ensure unipolar supply voltages

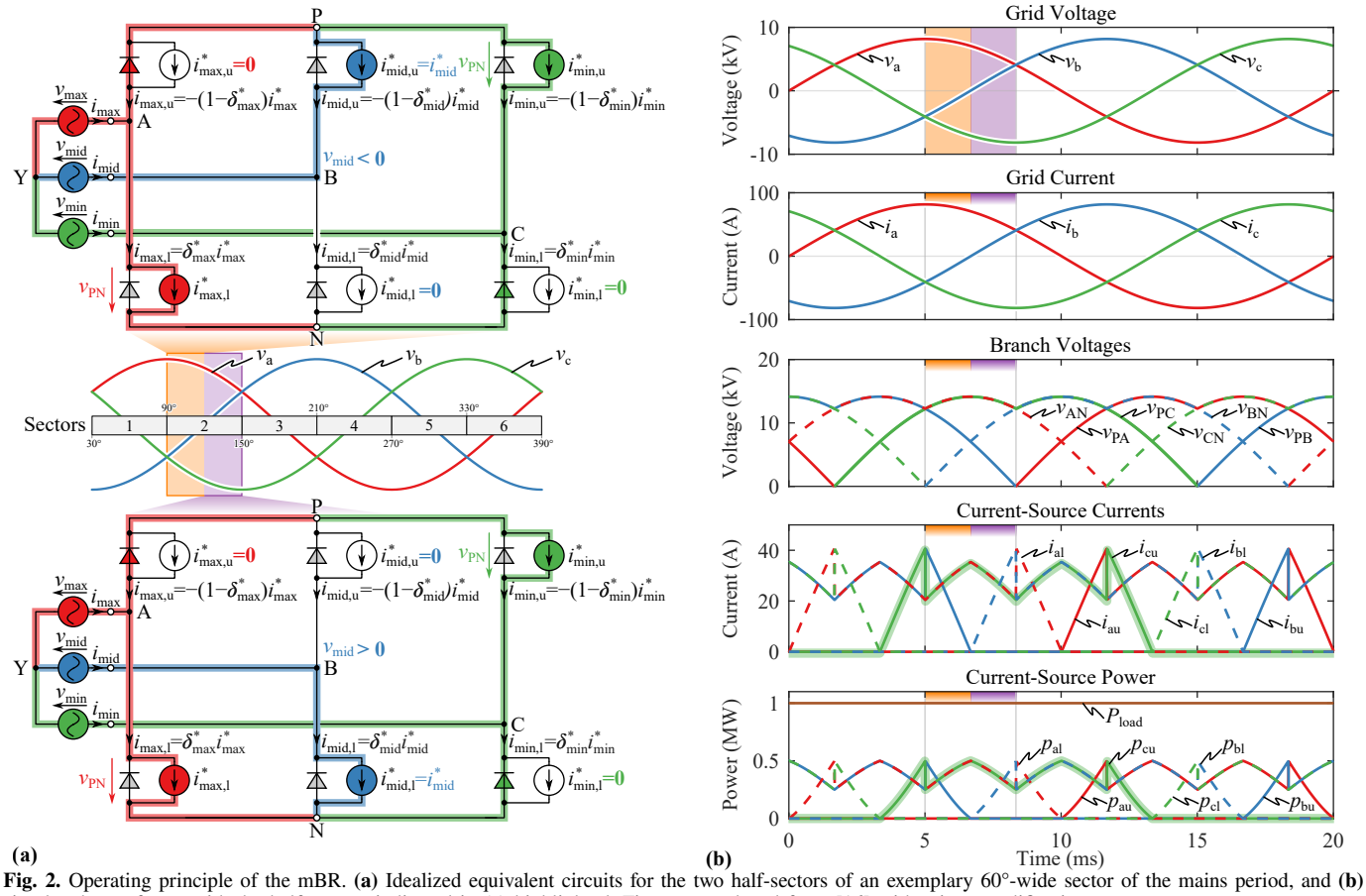

Fig. 2. Operating principle of the mBR. **(a)** Idealized equivalent circuits for the two half-sectors of an exemplary 60°-wide sector of the mains period, and **(b)** simulated waveforms with the half-sectors indicated in (a) highlighted. Figure reproduced from [16] with minor modifications.

at the inputs of the converter modules, i.e., essentially, the mBR replaces the ac-dc stage found in the converter cells of typical phase-modular SSTs with a single diode, similar to the approach from [21]. The mBR was proposed (but not explained) in [15], and later analyzed in [16] for the first time.

For convenience, this paper first recalls key aspects regarding the mBR operating principle from [16] and discusses the branch-level modeling approach in **Section II**. Then, **Section III** discusses the previously proposed branch-oriented current control method and its shortcomings. To overcome these deficiencies, **Section IV** introduces a novel analysis and current control method ("ΣΔ-Vector control"), which combines the well-known Clarke transformation and a specific ΣΔ decoupling. The new method improves the grid current tracking performance and facilitates mBR realizations with smaller branch inductors (L_{br} in **Fig. 1**), as is confirmed by simulation results in **Section V**. Finally, the **Appendix** discusses operational details and **Section VI** concludes the paper.

II. Modularized Bridge Rectifier

The mBR MVac-LVdc SST topology is shown in **Fig. 1**, and was originally proposed in [15], but only later analyzed in detail in [16]. The mBR can be derived from a three-phase (6-pulse) diode rectifier in which each functional diode is realized as a series connection of multiple diodes to withstand the high voltages of a MVac mains. Each diode (ideally) enforces a non-negative voltage across its terminals that serves as an unipolar input for isolated dc-dc converters connected in parallel. These dc-dc converters are configured in an input-series output-parallel (ISOP) arrangement (note that other output connections could be considered) and transfer power to the LVdc output.[1] The mBR consists thus of two triplets of star-connected output branches (OBs), each composed of N PEBBs connected in series on the input side and are tied to a mains phase. The so-called upper branches (indicated with u) connect to the P node, while the lower OBs (noted with l) to the N node, and each of the mains terminals A, B, and C connects to one upper and one lower branch. The mBR is thus fully modular, as the overall converter is obtained by replicating the same PEBB (consisting of a rectifier diode and an isolated dc-dc converter).

A. Operating Principle

Fig. 2 shows an idealized equivalent circuit of the mBR, where the OBs are replaced by controlled current sources, which is used to summarize the operating principle based on [16], where more detailed explanations are given. As a grid-tied converter, the mBR must control the mains currents i_a, i_b, and

[1] Note that we consider rectifier operation, i.e., power flow from the MVac mains to the LVdc output, but the mBR can, in principle and with certain circuit modifications also operate as an inverter [16].

i_c to the corresponding sinusoidal references i^*_a, i^*_b, and i^*_c to transfer power with a high power factor (PF). The OBs are controlled in such a way that the mains voltages v_a, v_b, and v_c define the conduction state of the diodes, thus dividing the grid period into six 60°-wide sectors. In each sector, the phase with the maximum (max) voltage is thus connected to P and the phase with the minimum (min) voltage to N; both diodes associated with the middle (mid) phase are blocking.

The current sources in parallel to blocking diodes see a positive voltage and hence can draw power, while the ones in parallel to conducting diodes cannot as their voltage is ideally zero. Thus, the first step in the analysis of the mBR consists in the mapping of the grid current references i^*_{max}, i^*_{mid}, and i^*_{min} into the branch current references, i.e., $i^*_{max,u}$, $i^*_{mid,u}$, and $i^*_{min,u}$ for the upper OBs, and $i^*_{max,l}$, $i^*_{mid,l}$, and $i^*_{min,l}$ for the lower ones; the desired current flow paths for two exemplary sectors are indicated in **Fig. 2a**. Finally, the branch current references are mapped back to $i^*_{a,u}$, $i^*_{b,u}$, $i^*_{c,u}$, $i^*_{a,l}$, $i^*_{b,l}$, and $i^*_{c,l}$ depending on the sector. This process is named "mBR references generation" and is the first step for both control methods.

To normalize the problem to the target grid current, the delta parameters can be introduced as the fraction of grid phase current that flows into the respective lower branch, e.g.,

$$\delta_{max} = \frac{i^*_{max,l}}{i^*_{max}} = 1 - \frac{i^*_{max,u}}{i^*_{max}}, \tag{1}$$

as shown in **Fig. 2a**. Due to the two star points P and N, the delta variables are linked by Kirchhoff's current law (KCL) as

$$\delta^*_{min} i^*_{min} + \delta^*_{mid} i^*_{mid} + \delta^*_{max} i^*_{max} = 0. \tag{2}$$

Hence, only two degrees of freedom (DoFs) are available for the choice of the δ variables, which are in turn functions of the grid angle θ. In the mid phase, the direction of the phase current defines whether the upper or the lower current source should be active, as only one option leads to the desired power flow direction (power drawn from the gird, i.e., absorbed by the current source), i.e., $\delta^*_{mid} = 0.5\,[1 + \mathrm{sgn}\,(v_{mid})]$ (assuming operation with unity PF and hence $i^*_{mid} \propto v_{mid}$). This behavior is clearly visible in **Fig. 2a**. Then, the one remaining DoF (i.e., either δ^*_{max} or δ^*_{min}) can be leveraged to equalize the power processing of the branches, which yields an analytical expression for the optimal $\delta^*_{max,opt}$ in dependence of the grid current references and hence of the grid angle (for details see [16]). The resulting (ideal) key waveforms are reported in **Fig. 2b**. Note that the discontinuities in the branch currents (references) at the sector boundaries are not realizable in an actual implementation due to bandwidth limitations. Hence, certain adaptions of the $\delta^*_{max,opt}$ can be used to obtain continuous current references (for details see [16]). In general, other optimization targets could possibly yield better results depending on the application and technology involved, but a more detailed discussion is beyond the scope of this paper.

B. Branch Modeling

Typical isolated dc-dc converter topologies (i.e., dual active bridge converters, or LLC-type converters) feature an input capacitor and hence cannot directly control their input current.

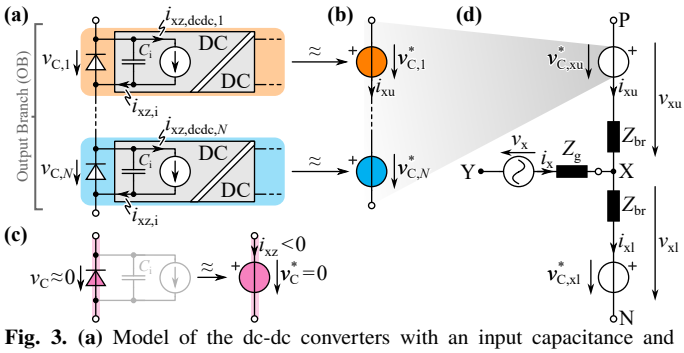

Fig. 3. (a) Model of the dc-dc converters with an input capacitance and impressed current. **(b)** Approximation of each power electronics building block (PEBB) as an equivalent voltage source v^*_C, as the dc-dc converter controls the voltage of its grid-facing capacitor C_i. **(c)** Detail of the approximation of a voltage generator acting as a diode. **(d)** Equivalent model of a generic phase x with a unified voltage source representing all the PEBBs of the branch.

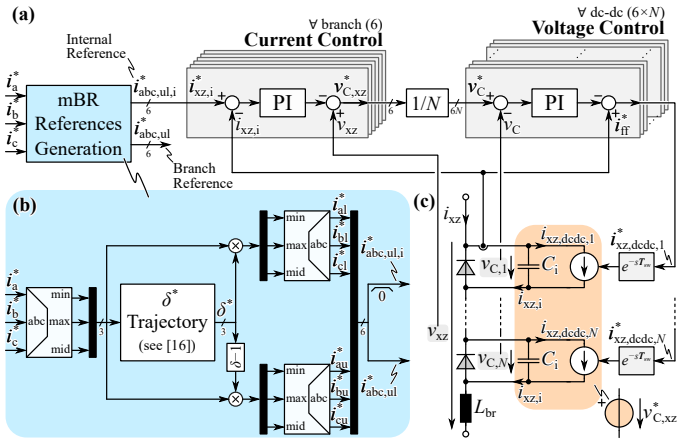

Fig. 4. Conventional control strategy for the mBR as proposed in [16]. **(a)** Block diagram of the branch-oriented current control, including **(b)** the calculation of the OB (i.e., internal) current references. **(c)** Model of one OB, in which the dc-dc converters are represented by CSs with an actuation delay of a switching period (e.g., typical for DAB-type converters) and an input capacitor.

Thus, whereas modeling the OBs with ideal current sources as above is helpful for explaining the operating principle, an actual implementation must realize a corresponding behavior by controlling the branch current in a branch inductor L_{br}, see **Fig. 1**, or, in more general terms, in branch impedance Z_{br}, via the OB input voltages. A first-order model of such dc-dc converters contains a grid-facing input capacitance C_i and an equivalent current source $i_{xz,dcdc}$ that represents the (controlled) power flow to/from the dc side of the converter, as shown in **Fig. 3a** [16]. By means of this current, each dc-dc converter can regulate the voltage v_C across its capacitor as can be seen by applying the Laplace transform to the KCL

$$i_{xz,i} = sC_i v_C + i_{xz,dcdc} \tag{3}$$

for a generic dc-dc converter in the branch z of phase x (where $i_{xz,i}$ is its input current, i.e., not including the diode current).

In the following, a sufficient control bandwidth is assumed for dc-dc converter's input voltages. Hence, the PEBB (i.e., the dc-dc converter and the diode) can be represented by an equivalent voltage source as shown in **Fig. 3b**; to ensure the validity of the model, the reference voltages must adhere to the working conditions of the anti-parallel diode, as depicted in **Fig. 3c**, i.e.,

$v_C^* \approx 0$ when the branch current $i_{xz} < 0$. Note that $v_C^* > 0$ can be enforced even for $i_{xz} < 0$, i.e., the blocking of the diode can be controlled by the dc-dc converter input voltage. However, this would result in a non-useful power transfer from the dc side to the ac side, because another branch would increase its power transfer from the ac side to counterbalance the former and maintain a constant power flow from the grid. Finally, the controlled voltages $v_{C,1}^*$, ..., $v_{C,N}^*$ representing the PEBBs of a branch can be aggregated into a single commanded voltage source $v_{C,xz}^*$ (for the generic branch z of phase x), as shown in **Fig. 3d** with the (inductive) branch impedances Z_{br} and the grid-side impedance Z_g.

III. Conventional Branch-Oriented Current Control

Based on the model described in **Section II-B**, it is possible to derive the straightforward branch-oriented current control algorithm [16] reported in **Fig. 4a**. The inputs are the grid current references i_a^*, i_b^*, and i_c^* that are generated by a higher-level control loop, e.g., to regulate the LVdc output voltage of the mBR, which is beyond the scope of this work. Then, the grid current references are mapped to the six OB current references $i_{xz,i}^*$ using the mBR reference generation via the δ^* variables as discussed in **Section II** and summarized in **Fig. 4b**. Considering one branch as shown in **Fig. 4c**, Kirchhoff's voltage law (KVL) expressed in the Laplace domain (note that the branch impedance is mainly inductive, i.e., $Z_{br} \approx sL_{br}$) is

$$v_{xz} = Z_{br} i_{xz} + v_{C,xz}^* \tag{4}$$

and serves as the basis for the branch-oriented control method from [16]. Intuitively, each branch current i_{xz} can be controlled with a dedicated PI controller via $v_{C,xz}^*$, i.e., via the dc-dc converters—however, the other branches act as a disturbance through v_{xz}. This effect can be mitigated by adding the measured value of v_{xz} as a feed-forward term to the PI controller output, as shown in **Fig. 4a**. If parameter uncertainty is not considered, $v_{C,xz}^*$ is equally actuated by the N dc-dc converters in each branch, each with reference $v_C^* = v_{C,xz}^*/N$. Inner regulation loops of the dc-dc converters track these input capacitor voltage references by adjusting the power transfer to the dc-side load (i.e., by adapting $i_{xz,dcdc}$. Again, to decouple the dynamics from the disturbances external to the dc-dc converter, the measured OB current $i_{xz,i}$ is added to the controller's output as a feed-forward term, as suggested by (3). As shown in **Fig. 4c**, the equivalent model of the dc-dc power stage consists of a controlled CS with a fixed actuation delay (corresponding to a switching period $T_{sw} = f_{sw}^{-1}$, where f_{sw} is the switching frequency of the dc-dc converter), which is a suitable representation of, e.g., DAB-type converters. Ultimately, from (3) and (4) it is straightforward to quantitatively design the regulators.

Although straightforward, the branch-oriented current control method can give poor results under certain operating conditions (as shown later in **Section V**). The main issue is that, essentially, *six* degrees of freedom (DOF), i.e., six branch currents, are controlled independently (hence the name "branch-oriented") even though the mBR circuit structure offers only *four* DOF, as can be seen in **Fig. 1**.[2] Besides, since the star-points P and N are not at a fixed potential, which is determined by the average between the voltages generated by their three branches, each branch current is also affected by the voltages applied to the other branches, i.e., there is a coupling between different branches. A decoupling effect is obtained via a voltage feed-forward, i.e., the measured branch voltage v_{xz} is used to compensate the disturbances caused by the other branches and the grid. The measurement of the branch voltages with sufficient bandwidth (see the idealized waveforms in **Fig. 2b**) is not trivial due to the MV levels. Finally, the branch-oriented control cannot directly consider any grid-side impedance Z_g [see (4)] that might, however, substantially affect control performance.

IV. Novel ΣΔ-Vector Current Control

The lack of coordination between the OBs in case of the conventional control method discussed above is solved in the proposed ΣΔ-Vector current control approach by means of the well-known Clarke transformation (also known as αβ-transformation) and a specific transformation named ΣΔ to control only the available *four* DOF in a decoupled fashion.

A. ΣΔ-*Vector Model*

As in **Section II-B** and **Fig. 3d**, each branch can be modeled as a single commanded voltage generator (assuming sufficient bandwidth of the inner dc-dc converter input voltage control loops), i.e., v_{au}, v_{bu}, v_{cu} for the upper branches and v_{al}, v_{bl}, v_{cl} for the lower branches. **Fig. 5a** shows the resulting equivalent circuit and introduces a compact notation (e.g., grid voltages v_a, v_b, and v_c are indicated with $v_{abc,g}$). Balanced impedances among the branches and the mains phases are assumed, i.e., all equal to Z_{br} and Z_g, respectively. Note that for now the rectifier diodes are not considered; finally, the correct conduction states can be ensured via a simple clamping method introduced later.

To simplify the analysis, the Laplace transform is applied in the following. For a generic phase x (a, b or c) and star-point Z (P or N), the KVLs result in

$$v_{xu}^* + Z_{br} i_{xu} + v_{xl}^* + Z_{br} i_{xl} = v_{PN}, \tag{5}$$

$$v_x - Z_g i_x + v_{YZ} = \mp (v_{xz}^* + Z_{br} i_{xz}). \tag{6}$$

Then, the application of the Clarke transform yields

$$v_{\alpha\beta,u}^* + Z_{br} i_{\alpha\beta,u} + v_{\alpha\beta,l}^* + Z_{br} i_{\alpha\beta,l} = 0 \text{ and} \tag{7}$$

$$v_{\alpha\beta,g} - Z_g i_{\alpha\beta,g} = \mp (v_{\alpha\beta,z}^* + Z_{br} i_{\alpha\beta,z}) \tag{8}$$

regarding the branches and the grid, respectively, where z is either the upper (u) or the lower (l) branch. Given the symmetry of the impedances connected to nodes P and N, the 0-component of the upper- and lower-branch generators does not affect the αβ branch currents, as shown by (7) or by applying Millman's theorem. Moreover, the related 0-component current cannot flow in any of the triplets star-connected to P, N, and

[2]The mBR consists of three three-phase systems (the grid, the upper, and the lower OBs) with respective star points Y, P, and N, which are interconnected at the three common nodes A, B, and C. Thus, there are nine current variables as potential DOF (three grid currents, six branch currents) but also six nodes that, via the KCL, give six constraints. One of these is a linear combination of the others, and hence 9 – 5 = 4 independent current variables remain as DOF.

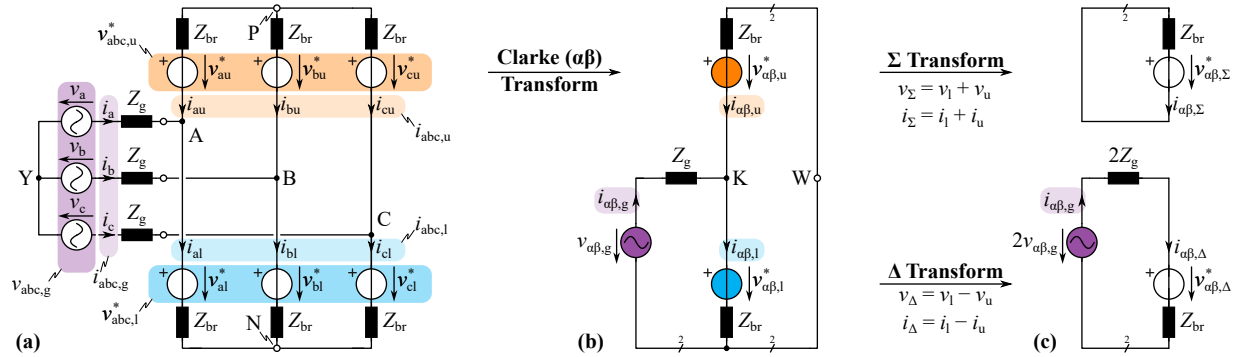

Fig. 5. **(a)** Equivalent circuit of the mBR with branches (i.e., series-connected dc-dc converters) operating as controlled voltage sources as in **Fig. 3**. Applying the Clarke transformation leads to **(b)** the equivalent circuits for α and β (superimposed for the sake of a compact representation). **(c)** Using a ΣΔ transformation advantageously further simplifies the circuit and facilitates a decoupled analysis of the sum (Σ) and the difference (Δ) of the branch voltages in αβ coordinates as the remaining *four* control variables; again, the circuit for α and β coordinates are superimposed.

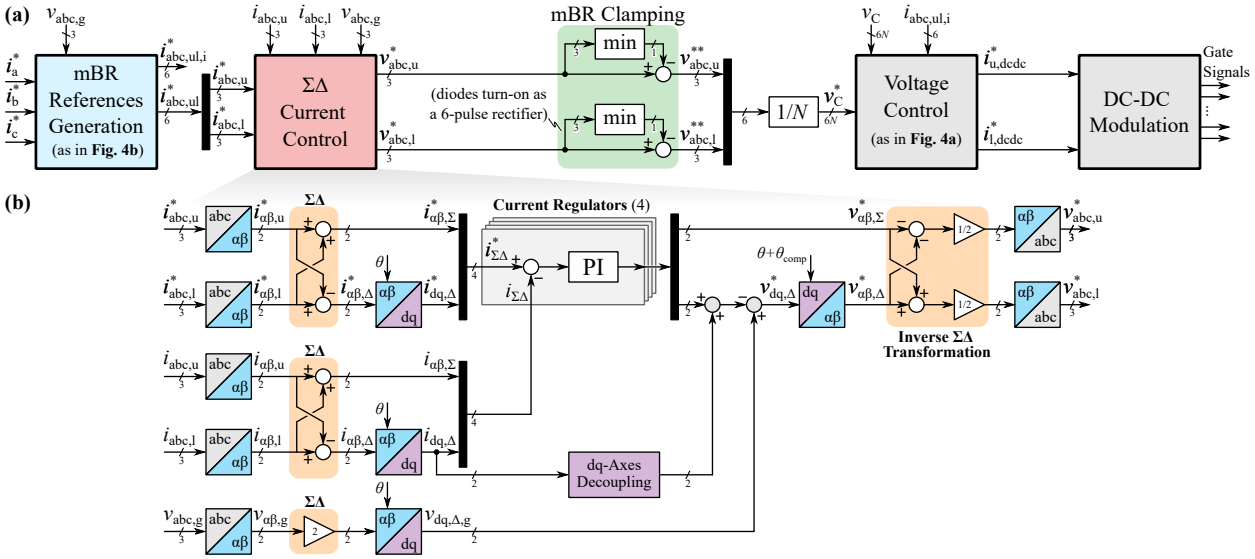

Fig. 6. Proposed ΣΔ-Vector current control based on the model in **Fig. 5**. **(a)** High-level overview and **(b)** detailed block diagram of the core of the novel ΣΔ-Vector current control, in which the proposed ΣΔ decoupling, together with Clarke and dq transformations, ensures coordination between the different branches and ultimately only the effectively available *four* DOF are controlled ($i^*_{\alpha\beta,\Sigma}$ and $i^*_{\alpha\beta,\Delta}$ each are vectors of length 2). Note that the "mBR clamping" ensures the desired diode operation by leveraging the 0-component of the Clarke transform, which does not influence the current in the αβ coordinates.

Y. Therefore, the 0-component voltages are excluded from the analysis of current control, but will be leveraged later to ensure that the diode conduction states advantageously correspond to those of a 6-pulse rectifier (see **Section II-B**).

The resulting equivalent circuit is reported in **Fig. 5b** where, matching the actual number of DOF, only *four* controlled variables remain ($i_{\alpha\beta,u}$ and $i_{\alpha\beta,l}$, each a vector of lenght 2; $v_{\alpha\beta,g}$ follows from the KCL at node K). However, each of the two controlled voltage sources $v_{\alpha\beta,u}$ and $v_{\alpha\beta,l}$ still influences both currents, as can be easily seen from (7). As this coupling reduces performance (or, alternatively, requires a more complex controller), an additional transformation of the control variables is introduced to decouple them entirely. In particular, it is advantageous to consider the sum (Σ) and the difference (Δ) of the branch voltage references, i.e.,

$$v^*_{\alpha\beta,\Sigma} \overset{\text{def}}{=} v^*_{\alpha\beta,l} + v^*_{\alpha\beta,u} \tag{9a}$$

$$v^*_{\alpha\beta,\Delta} \overset{\text{def}}{=} v^*_{\alpha\beta,l} - v^*_{\alpha\beta,u}. \tag{9b}$$

The corresponding inverse transformation is therefore

$$v^*_{\alpha\beta,l} = \frac{1}{2}\left(v^*_{\alpha\beta,\Sigma} + v^*_{\alpha\beta,\Delta}\right) \tag{10a}$$

$$v^*_{\alpha\beta,u} = \frac{1}{2}\left(v^*_{\alpha\beta,\Sigma} - v^*_{\alpha\beta,\Delta}\right). \tag{10b}$$

The substitution of (10a) and (10b) in (7) and (8) yields

$$v^*_{\alpha\beta,\Sigma} = -Z_{\text{br}}\left(i_{\alpha\beta,l} + i_{\alpha\beta,u}\right) \quad \text{and} \tag{11}$$

$$v^*_{\alpha\beta,\Delta} = -\left(Z_{\text{br}} + 2Z_{\text{g}}\right)\left(i_{\alpha\beta,l} - i_{\alpha\beta,u}\right) + 2v_{\alpha\beta,\text{g}}\,, \tag{12}$$

respectively. This leads to the convenient definition of

$$i_{\alpha\beta,\Sigma} \overset{\text{def}}{=} i_{\alpha\beta,l} + i_{\alpha\beta,u} \tag{13a}$$

$$i_{\alpha\beta,\Delta} \overset{\text{def}}{=} i_{\alpha\beta,l} - i_{\alpha\beta,u}. \tag{13b}$$

Note that the transformed variable $i_{\alpha\beta,\Delta}$ corresponds to the grid current, i.e., $i_{\alpha\beta,\Delta} = i_{\alpha\beta,\text{g}}$. With (11) and (12) we have

$$i_{\alpha\beta,\Sigma} = -\frac{v^*_{\alpha\beta,\Sigma}}{Z_{\text{br}}} \quad \text{and} \tag{14}$$

$$i_{\alpha\beta,\Delta} = -\frac{v^*_{\alpha\beta,\Delta} - 2v_{\alpha\beta,\text{g}}}{Z_{\text{br}} + 2Z_{\text{g}}}. \tag{15}$$

Ultimately, Σ and Δ quantities are fully decoupled, i.e., $i_{\alpha\beta,\Sigma}$ depends on $v^*_{\alpha\beta,\Sigma}$ only and $i_{\alpha\beta,\Delta}$ depends on $v^*_{\alpha\beta,\Delta}$ only, which is captured by the equivalent circuits shown in **Fig. 5c**.

B. ΣΔ-Vector Control Strategy

A novel control strategy based on the decoupled equivalent circuits shown in **Fig. 5c** is proposed in the following.

1) Control Diagram: **Fig. 6a** shows the high-level diagram of the new control method. Similarly to the previous approach (**Fig. 4**), the mains current references i^*_a, i^*_b, and i^*_c represent the inputs; however, these are mapped to the six branch current references $i^*_{abc,ul}$ instead of the OB (internal) references $i^*_{abc,ul,i}$ as in the branch-oriented control (the main difference being that $i^*_{abc,ul}$ also encompass the diode currents). Then, as depicted in **Fig. 6b**, the Clarke and ΣΔ transformations are applied to the six branch current references $i^*_{abc,ul}$ to obtain two sets of transformed references $i^*_{\alpha\beta,\Sigma}$ and $i^*_{\alpha\beta,\Delta}$. Similarly, the measured branch currents $i_{abc,ul}$ are transformed to $i_{\alpha\beta,\Sigma}$ and $i_{\alpha\beta,\Delta}$.

Since $i_{\alpha\beta,\Delta} = i_{\alpha\beta,g}$, the α and β components of $i^*_{\alpha\beta,\Delta}$ are sinusoidal at the grid frequency and, hence, it is beneficial to apply a dq transform (i.e., the rotating reference frame aligned with the grid voltage $v_{\alpha\beta,g}$, defined by the grid angle θ) to both the references $i^*_{\alpha\beta,\Delta}$ and the measured values $i_{\alpha\beta,\Delta}$.[3] Thus, $i^*_{dq,\Delta}$ and $i_{dq,\Delta}$ are obtained, respectively.

Then, there are *four* PI regulators (not six as in the branch-oriented control) acting on the transformed current references and measurements. For the dq-Δ components, as the impedance in (15) is (mainly) inductive, it is beneficial to implement the standard decoupling of the d- and q-axis [22]. The (transformed) measured grid voltage $v_{dq,\Delta,g}$ is added as a feed-forward [as indicated by (15)]. Advantageously, the three grid voltages can be measured with only low bandwidth requirements, whereas measuring the six branch voltages used in the conventional control method requires high bandwidth, i.e., is more complicated/expensive. Furthermore, the inverse dq transform is applied with a phase advancement θ_{comp} equal to the delay introduced by the limited-bandwidth voltage control for its compensation [22]. Finally, the inverse ΣΔ transform (10) and the inverse Clarke transformation are applied to obtain the six voltage references for the upper and lower branches.

2) mBR Clamping: As discussed in **Section II-B**, it is advantageous to ensure that the diode rectifier conduction state corresponds to that of a standard 6-pulse rectifier (i.e., the diodes of the upper branch connected to the max phase and the diodes of the lower branch connected to the min phase conduct, as in **Fig. 3c**). This can be ensured by leveraging the 0-component of the upper and lower branch voltages, which does not interfere with the branch current control (see **Section IV-A**). Specifically, the minimum of all three voltage references of the upper branches is subtracted as a common offset (0-component) from all three references, clamping the minimum reference to zero, i.e., the one corresponding to the branch that should conduct current through the diodes; the lower branches are treated likewise as indicated in **Fig. 6a**. Finally, the voltage references $v^{**}_{abc,ul}$ obtained after the clamping are then distributed to and controlled by the individual dc-dc converters as in the branch-oriented control strategy (**Section III**, **Fig. 4**).

3) Grid Voltage Feed-Forward: The grid voltage represents a strong disturbance to the current control loops, since its magnitude is very large compared to the voltage drop across branch inductance, making the relative feed-forward necessary for mitigating this effect on grid current. Both the imperfect measurement of mains-voltage and the voltage actuation delay may lead to significant control errors on grid current. The dq transformation is thus beneficial, as it achieves quasi-zero error at the synchronous frequency (i.e., at the mains frequency), even with non-ideal feed-forward, thanks to the integral gain of the regulator. A noteworthy difference subsists with the branch-oriented method, in which the feed-forward is used as a decoupling action adding the branch voltage v_{xz} that, however, depends on the control action (i.e., the dc-dc converter's voltage) of the same branch, yielding an imperfect decoupling.

V. Simulation Results

Detailed circuit simulations are used to evaluate the proposed ΣΔ-Vector current control method for the mBR, considering the transfer of 1 MW of power from a 10 kV (line-to-line rms) MVac grid. The equivalent circuit for the dc-dc converters shown in **Fig. 4c** is used with input capacitors $C_i = 1.2\,\mu F$, branch inductors $L_{br} = 1\,mH$, and inductive Z_g with $L_g = 15\,mH$. **Fig. 7** shows the regulation performance of the ΣΔ-Vector control, where a reference step is introduced for the grid current at 13.1 ms and a 10 % step in the grid voltage happens at 38.3 ms. Whereas a good tracking of the grid current references is achieved in the dq reference frame (i.e., Δ-dq currents), the same is not attainable for the Σ currents controlled in the αβ reference frame (i.e., Σ-αβ) due to the higher harmonic content and the limited control bandwidth (670 Hz for the considered specifications, using (15) and (14) with a simple zero-pole cancellation). Note, however, that a different selection of the δ^* parameters could be employed to reduce the steepness the piece-wise linear branch current reference waveforms at the price of possibly higher rms currents (see **Section II-A** and [16]), relaxing the control bandwidth requirements.

A comparison between the conventional branch-oriented current control and the proposed ΣΔ-Vector current control strategy is shown in **Fig. 8**. The operation is first shown for an mBR with the same parameters as in **Fig. 7** except for $L_{br} = 10\,mH$. The current references are increased from zero to 60% and then to 100%. Both control strategies are able to properly regulate the grid current, but the ΣΔ-Vector strategy performs slightly better with a total harmonic distortion (THD) of 0.20% and a steady-state phase error of 0.05° (on the fundamental), compared to the 0.68% THD and 0.6° phase error of the conventional control (besides, see also the difference in the first 10 ms of **Fig. 8a**). Then, the mBR is restarted at 70 ms but smaller branch inductors $L_{br} = 1\,mH$ are considered in the simulation *ceteris paribus* (all the other parameters are the same; note that the regulator gains are adapted to the new L_{br} value). Ultimately, even though not completely unstable,

[3] As the Σ components are not sinusoidal, the opportunity of applying a dq transform to these variables was not investigated, but could still be beneficial.

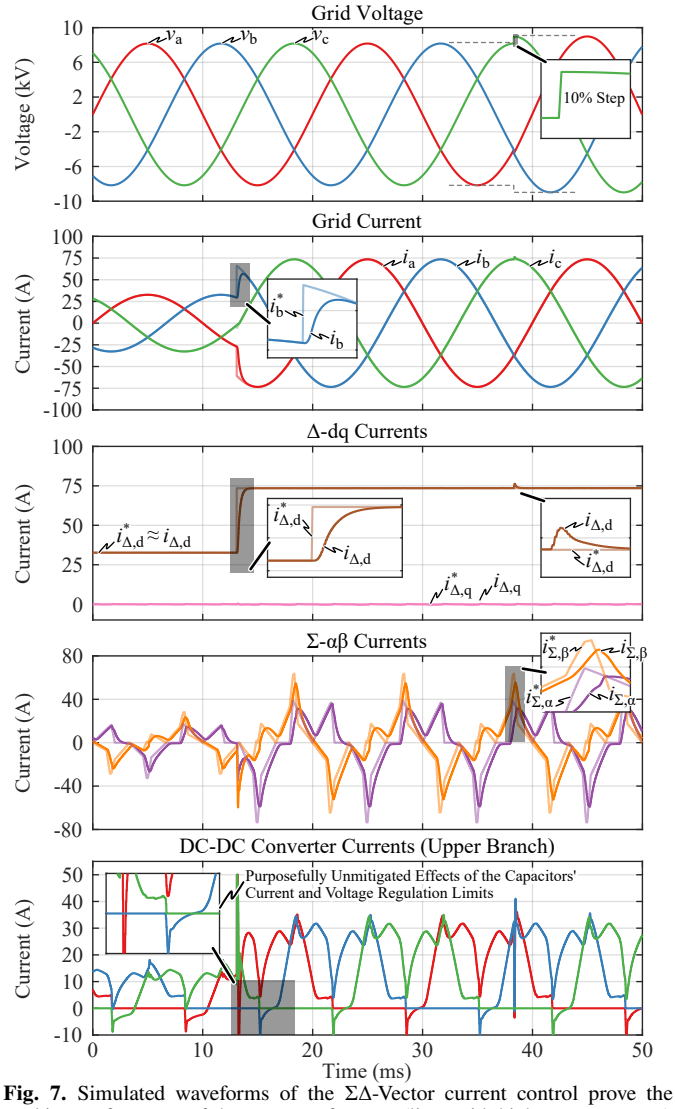

Fig. 7. Simulated waveforms of the ΣΔ-Vector current control prove the tracking performance of the current references (lines with higher transparency). The dynamic response is highlighted for a step increment of the mains current references (which correspond to the Δ-dq currents) at 13.1 ms, and for a +10 % step of the grid voltage amplitude at 38.3 ms. The last tile shows purposely unmitigated effects regarding the dc-dc converters' operation (see **Appendix**).

the conventional branch-oriented control does not achieve a satisfactory regulation of the grid currents, whereas the novel ΣΔ-Vector control strategy achieves again very good tracking of the grid references with very low distortion. Thus, the proposed method shows to be more robust and, in particular, facilitates much smaller branch inductors, i.e., lower realization effort.

VI. Conclusion

A recent publication [16], has presented the first analysis of a new concept by [15] for MVac-to-LVdc solid-state transformers (SSTs), called modularized bridge rectifier (mBR). The only previously published control strategy, [16], is of branch-oriented nature, i.e., tries to regulate each of the six branch currents independently, but this is not ideal due to strong coupling between the branches as a consequence of the circuit structure. Therefore, this paper contributes a new modeling and control strategy for the mBR: the proposed ΣΔ-Vector method employs the Clarke transformation and a new decoupling (ΣΔ) transformation to regulate the three grid currents and the six branch currents using only the four effectively available degrees of freedom. Detailed circuit simulations show that, compared to the conventional branch-oriented control method, the new ΣΔ-Vector control leads to improved performance and robustness to parameters variation thanks to the coordination between the branches and the full decoupling of control variables.

Future work should address the improvement of low-voltage operation of the branches (see **Appendix**), the reduction of the passive elements, and in-depth analyses on the impact of mBR trajectories on the control and design, which would lead to a more comprehensive optimization (e.g., including dc-dc operation, reactive components design, and the trade-off between the control bandwidth requirements and decreased rms current resulting from a steep trajectory [16]), possibly using smooth trajectories that yield current references with continuous derivative (i.e., without cusps).

Appendix – Details About MBR Operation

In the novel ΣΔ-Vector control, the "mBR clamping" ensures a null voltage reference for the branch that should present diode conduction, whereas this is not strictly enforced in the branch-oriented approach. Besides, while a diode is conducting, its current is actively and coordinately controlled by the other branches thanks to the αβ transformation. Alas, depending on the chosen δ trajectory, the involved dc-dc converters (i.e., the branch) may operate with a low grid-side voltage, i.e., more difficult control and reduced efficiency. The same occurs when a branch is decreasing its voltage towards a diode commutation (see v_{PC} near 15 ms in **Fig. 2b**). In addition, the dc-dc converter's operation is complicated also by the low-frequency current induced by the grid into its capacitor, which peaks at $\pm 2\pi f_g C_i V_{g,pk}/N$ (with ideal waveforms as in **Fig. 2b**, f_g as the mains frequency, and $V_{g,pk}$ as the peak line-to-line grid voltage); this current will be compensated by the voltage regulator, as shown in the last tile of **Fig. 7**. In other words, to have a unity grid PF, the regulators compensate for the equivalent reactive current that would flow if the dc-dc converters were turned off, hence, substantially modifying their operating point, and, especially at low voltage, possibly inducing a negative current sinking (see **Fig. 7**), i.e., inverted power flow. Ultimately, the impact of these currents is determined by the mBR trajectory and the ratio between f_g and f_{sw} (the latter, due to the voltage ripple, determines the lower bound on C_i).

Furthermore, different strategies can tackle the problem of low-voltage operation of dc-dc converters. The voltage controllers and the dc-dc converters could be turned off at a certain voltage threshold if the power transfer is not required, [16]. Alas, an undesired current is then injected into the branch via the L_{br}-C_i path by the varying voltages (see **Fig. 2b**) that come about across it. Another idea is to operate a reduced number of dc-dc modules when the desired branch voltage is low; however, many implementation details are to be considered, e.g., changing the activation sequence to equally distribute

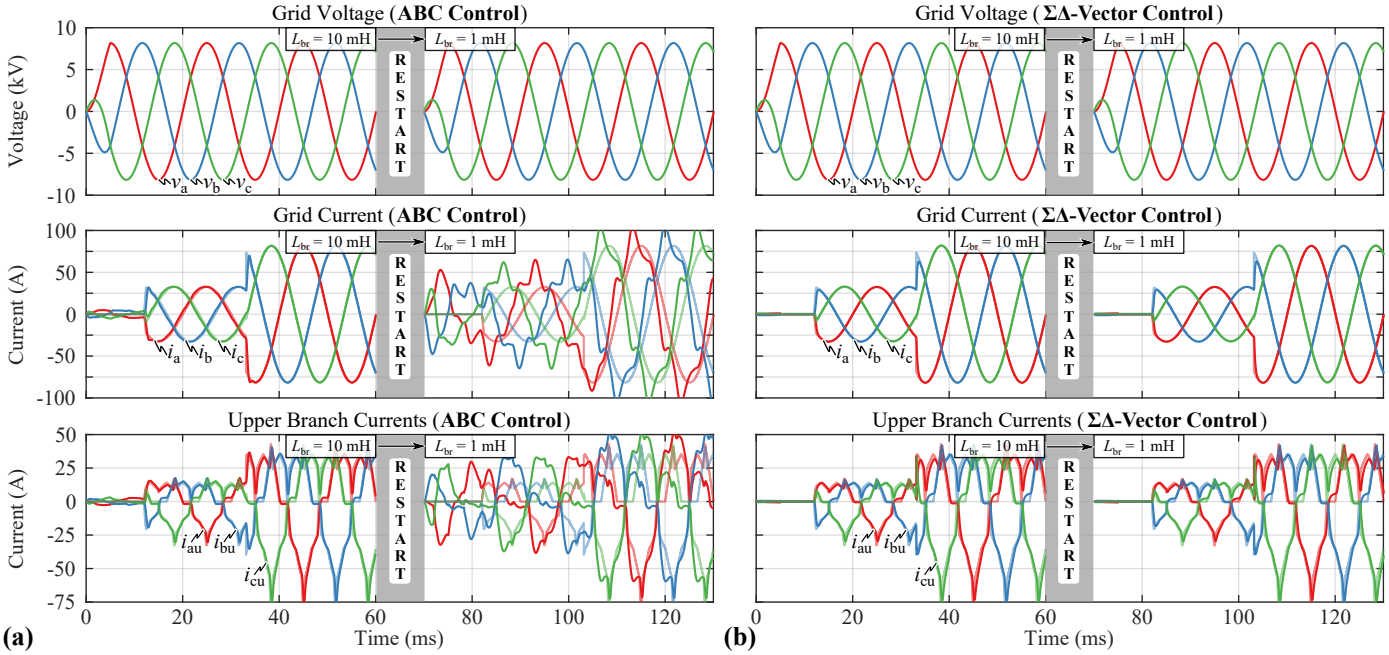

Fig. 8. Comparison of the mBR operated with **(a)** the branch-oriented control and **(b)** the ΣΔ-Vector control. The simulations show two consecutive steps of current references with inductive Z_g equal to $L_g = 15\,\text{mH}$ and branch inductor $L_{br} = 10\,\text{mH}$. Both control strategies are able to properly regulate the grid current, but the ΣΔ-Vector strategy performs slightly better. Then, the mBR is turned off at 60 ms and restarted at 70 ms with lower $L_{br} = 1\,\text{mH}$ (i.e., lower volume and cost) and regulators are accordingly retuned, but only the new ΣΔ-Vector control is able to regulate the grid current with low distortion.

losses, and whether the capacitors of the inactive PEBBs should be bypassed using dc-dc converter's switches (see [16]).

References

[1] M. Liserre, M. A. Perez, M. Langwasser, C. A. Rojas, and Z. Zhou, "Unlocking the hidden capacity of the electrical grid through smart transformer and smart transmission," *Proc. IEEE*, vol. 111, no. 4, pp. 421–437, 2023.

[2] N. Djekanovic and D. Dujic, "Design optimization of a MW-level medium frequency transformer," in *Proc. Inter. Exhib. Conf. Power Electron., Intell. Motion, Renewable Energy and Energy Manage. (PCIM Europe)*, Nuremberg, Germany, 2022.

[3] D. Dujic, F. Kieferndorf, F. Canales, and U. Drofenik, "Power electronic traction transformer technology," in *Proc. 7th Inter. Power Electron. Motion Control Conf.*, vol. 1, 2012, pp. 636–642.

[4] X. She, A. Q. Huang, and R. Burgos, "Review of solid-state transformer technologies and their application in power distribution systems," *IEEE J. Emerg. Sel. Topics Power Electron.*, vol. 1, no. 3, pp. 186–198, Sep. 2013.

[5] C. Zhao *et al.*, "Power electronic traction transformer—medium voltage prototype," *IEEE Trans. Ind. Electron.*, vol. 61, no. 7, pp. 3257–3268, Jul. 2014.

[6] S. Srdic and S. Lukic, "Toward extreme fast charging: Challenges and opportunities in directly connecting to medium-voltage line," *IEEE Electrific. Mag.*, vol. 7, no. 1, pp. 22–31, Mar. 2019.

[7] W. Xu, S. Rajendran, Z. Guo, A. Vetrivelan, and A. Q. Huang, "13.8kV/400kW solid state transformer DC fast charger (SST-DCFC) based on 15kV SiC AC switch," in *Proc. IEEE Energy Convers. Congr. Expo. (ECCE USA)*, Nashville, TN, USA, 2023, pp. 905–912.

[8] R. De Seram, K. T. Lulbadda, T. Sidhu, and S. S. Williamson, "A solid state transformer-based charging station for catering heavy/medium and light electric vehicles," in *Proc. 4th Int. Conf. Smart Grid Renewable Energy (SGRE)*, Doha, Qatar, 2024.

[9] K. Nakatsu, T. Kumazaki, A. Kanouda, K. Ide, and T. Tsukishima, "Development of smart power management for achieving carbon neutrality by 2050: Energy ccosystems for widespread EV adoption," *Hitachi Rev.*, vol. 71, no. 1, pp. 51–57, 2022.

[10] C. Zhu, "High-efficiency, medium-voltage-input, solid-state-transformer-based 400-kW/1000V/400A extreme fast charger for electric vehicles," U.S. Dept. Energy Office Sci. Tech. Inf., Tech. Rep. EE-0008361, Jul. 2023. [Online]. Available: https://www.osti.gov/servlets/purl/1987553/

[11] J. Huber, P. Wallmeier, R. Pieper, F. Schafmeister, and J. W. Kolar, "Comparative evaluation of MVAC-LVDC SST and hybrid transformer concepts for future datacenters," in *Proc. Int. Power Electron. Conf. (IPEC/ECCE Asia)*, Himeji, Japan, May 2022, pp. 2027–2034.

[12] R. Unruh, F. Schafmeister, N. Froehleke, and J. Boecker, "1-MW full-bridge MMC for high-current low-voltage (100V-400V) DC-applications," in *Proc. Power Convers. Intell. Motion Conf. (PCIM Europe)*, Nuremberg, Germany, Jul. 2020.

[13] Z. Li, R. Mirzadarani, M. Ghaffarian Niasar, M. Itraj, L. van Lieshout, P. Bauer, and Z. Qin, "Medium-voltage solid-state transformer design for large-scale H_2 electrolyzers," *IEEE Open J. Power Electron.*, vol. 5, pp. 936–955, 2024.

[14] S. S. Queiroz and L. F. Costa, "Design of a modular multilevel DC/DC converter to solid-state transformer in a green hydrogen system," in *Proc. IEEE Appl. Power Electron. Conf. Expo. (APEC)*, Long Beach, CA, USA, 2024, pp. 2282–2288.

[15] S. Götz, "Charging apparatus with a phase unit having multiple strands," US Patent US 10 439 407 B2, Oct., 2019.

[16] G. Andrioli, S. Calligaro, R. Petrella, J. W. Kolar, and J. Huber, "Analysis and comparative evaluation of a modularized bridge rectifier mvac-lvdc solid-state transformer," in *Proc. IEEE 10th Int. Power Electron. Motion Control Conf. (IPEMC-ECCE Asia)*, Chengdu, China, May 2024, pp. 2722–2729.

[17] W. van der Merwe and T. Mouton, "Solid-state transformer topology selection," in *Proc. IEEE Int. Ind. Techn. Conf. (ICIT)*, Gippsland, VIC, Australia, Feb. 2009.

[18] M. Hartmann, "Gleichrichterschaltung (in German)," Austria Patent AT 516 643 B1, Feb., 2018.

[19] M. Makoschitz, "Unidirectional medium voltage rectifier utilizing sinusoidal input currents," *Electron. Lett.*, vol. 58, no. 12, pp. 474–476, 2022.

[20] J. Huber, U. Drofenik, F. Canales, and J. W. Kolar, "Comparative evaluation of three-phase-unfolder-based MVAC-LVDC solid-state transformers," in *Proc. Power Convers. Intell. Motion Conf. (PCIM Europe)*, Nuremberg, Germany, 2024.

[21] R. Raju, "AC solid-state transformer with DC-DC converters," US Patent US11 811 301B1, Sep., 2023.

[22] B. H. Bae and S. K. Sul, "A compensation method for time delay of full-digital synchronous frame current regulator of pwm ac drives," *IEEE Trans. Ind. Appl.*, vol. 39, no. 3, pp. 802–810, 2003.